Synergistic retrievals of ice in high clouds from lidar, Ku-band radar and submillimeter wave radiometer observations

Mircea Grecu[a,b] and John Yorks [a]

[a] *NASA GSFC*

[b] *Morgan State University*

Corresponding author: Mircea Grecu, mircea.grecu-1@nasa.gov

ABSTRACT: Enter the text of your abstract here.

1. Introduction

The future NASA Atmospheric Observing System (AOS) mission (Braun 2022) is expected to feature new combinations of observations that may be used to quantify the amounts of ice in high clouds and characterize the microphysical properties of ice particles. These observations include lidar backscatter, Ku-band radar reflectivity and submillimeter wave radiometer brightness temperature measurements. While not optimal for cloud ice estimation, but for the characterization of a broader spectrum of cloud and precipitation processes, these observations are nevertheless synergistic from the characterization of ice clouds perspective. That is, despite the fact that lidar observations attenuate quickly in thick ice clouds and the Ku-band radar will not be able to detect clouds characterized by an echo weaker than 8.0 dBZ, the active observations are expected to provide context that may be incorporated into radiometer retrievals. Herein, term retrieval is defined as the process of estimating geophysical variables from remote sensing observations. In this study, we investigate the impact of incorporating the lidar and radar observations into the radiometer retrieval of ice clouds. Because the existent amount of coincident backscatter lidar, Ku-band radar, and submillimeter-wave radiometer observations is rather insufficient to derive conclusive results, we employ accurate physical models to simulate the lidar, radar and radiometer observations and use a cross-validation methodology to characterize the retrieval accuracy. As estimates from passive instrument observations strongly depend on the ”a priori” information (Rodgers 2000), for results to be relevant in real applications it is necessary to base them on realistic vertical distributions of ice properties. Such distributions may be derived from cloud-resolving-model (CRM) simulations (Pfreundschuh et al. 2020) or directly from observations. In this study, we employ the latter approach, as CRMs may still be deficient in properly reproducing the vertical distribution of ice clouds and their associated microphysical properties. Specifically, we use observation and products from the CloudSat (CS) mission (Stephens et al. 2002) to derive a database of ice microphysical properties and associated simulated lidar, radar and radiometer observations. The database is used to investigate the accuracy of the estimated ice cloud properties from the simulated observations. The article is organized as follows. In Section 2, we describe the approach used to derive the ice properties and the associated simulated observations, the retrieval and the evaluation methodology. In Section 3, we present the results of the evaluation methodology. We conclude in Section 4.

2. Methodology

As previously mentioned, we use CloudSat (CS) observations (Stephens et 2002) to derive the vertical distributions of ice properties needed in the investigation. Although research quality CS cloud ice products exist, to maximize the physical consistency of the approach, we do not use them but derive ice amounts and associated properties directly from CS reflectivity observations. This ensures the consistency between the particle distribution assumptions and the electromagnetic scattering properties used in the CS reflectivity processing and those used the simulation of the lidar, Ku-band radar and radiometer observations. Lidar, Ku-band radar and submillimeter-wave radiometer observations are simulated from CS observations using accurate physical models and realistic assumptions consistent with the most recent knowledge in the field of ice cloud microphysics, and a non-parametric estimation methodology based on the k-Means clustering algorithm MacKay (2003) is used to investigate the instrument synergy. Details of the methodology are presented below.

a. Assumptions and forward models

To quantify the number of ice particles in an elementary atmospheric volume as a function of their size, we use normalized gamma functions (Bringi et al. 2003). The benefit of normalized gamma functions is that they encapsulate the variability of Ice Water Content (IWC) - reflectivity relationship into a single parameter, i.e. the normalized Particle Size Distribution (PSD) intercept (Testud et al. 2001; Bringi et al. 2003). The normalized PSD intercept is defined as $N_w = \frac{4^4}{\pi \rho_w} \frac{IWC}{D_m^4}$, where IWC is the ice water content associated with the PSD, and D_m is the mass weighted mean diameter. Testud et al. (2001) showed that the variability in IWC reflectivity (Z) relationships may be fully explained by variability in N_w, and that a formula of the type

$$IWC = N_w^{1-b} a Z^b \tag{1}$$

perfectly explains the relationships between IWC and Z calculated from observed PSDs. Equation (1) is not sufficient to derive accurate, unbiased estimates of ice water contents, because N_w varies considerably in time and space. Nevertheless, multiple studies showed that it is beneficial to parameterize N_w as a function of various variables, such as temperature (e.g. Hogan et al.

2006; Delanoe and Hogan 2008; Deng et al. 2010), rather than using N_w independent relations. In this study, we parameterize N_w as a function of temperature based on the CloudSat 2C-ICE product (Deng et al. 2010; Deng et al. 2013). Specifically, we cluster, based on similarity, a large set 2C-ICE profiles into 18 classes using a k-Means procedure. The mean IWC profiles associated with the 18 classes are shown in continuous lines in Figure 1. Alternative estimates, derived using PSD assumptions and electromagnetic scattering calculations that enable accurate and physically consistent simulations of radar observations at Ku-band and radiometer observations of submillimeter-wave frequencies are also shown in Figure 1. These estimates are based on the self-similarity Rayleigh-Gans approximation (SSRGA) of Hogan et al. (2017). Details regarding the estimation process are provided in the following paragraphs. As apparent in Figure 1, the CS and SSRGA estimates are in good agreement. Some discrepancies due to differences between the SSRGA N_w parameterization and the CS 2C-ICE ”a priori assumptions” are also apparent, but they are not deemed critical in this study, whose objective is the investigation of synergistic lidar, Ku-band radar and submillimeter-wave radiometer retrievals, because the outcome is not likely to be sensitive to such details. One may notice that the average IWC profiles in Figure 1 are characterized by different peak values and heights. This facilitates a simple way to reverse-engineer to (some extent) the ”a priori” assumptions used in the CS 2C-ICE product and use them in formulation of the type described in Equation (1). Specifically, the derivation of relationships of the type $IWC = a_i Z^{b_i}$ for every class i may be used to study a_i as a function of height. Shown in Figure 2 is a representation of the class multiplicative coefficient a_i as a function of relative height scatter plot. As apparent in the figure, and as expected, a_i exhibits a strong variation with the relative height. Coefficient b_i exhibits a height dependency as well (not shown), but the range of variation is significantly smaller, almost zero relative to the mean value of b. Given that any deviation of the multiplicative coefficient in an IWC-Z relation from an average is equivalent to a deviation of the associated N_w from its mean value (Testud et al. 2001), the variation of a as a function of relative-height may be converted into a N_w as a function of relative-height relationship. We, therefore, use the data in Fig. 2 to parameterize N_w as a function of the relative height.

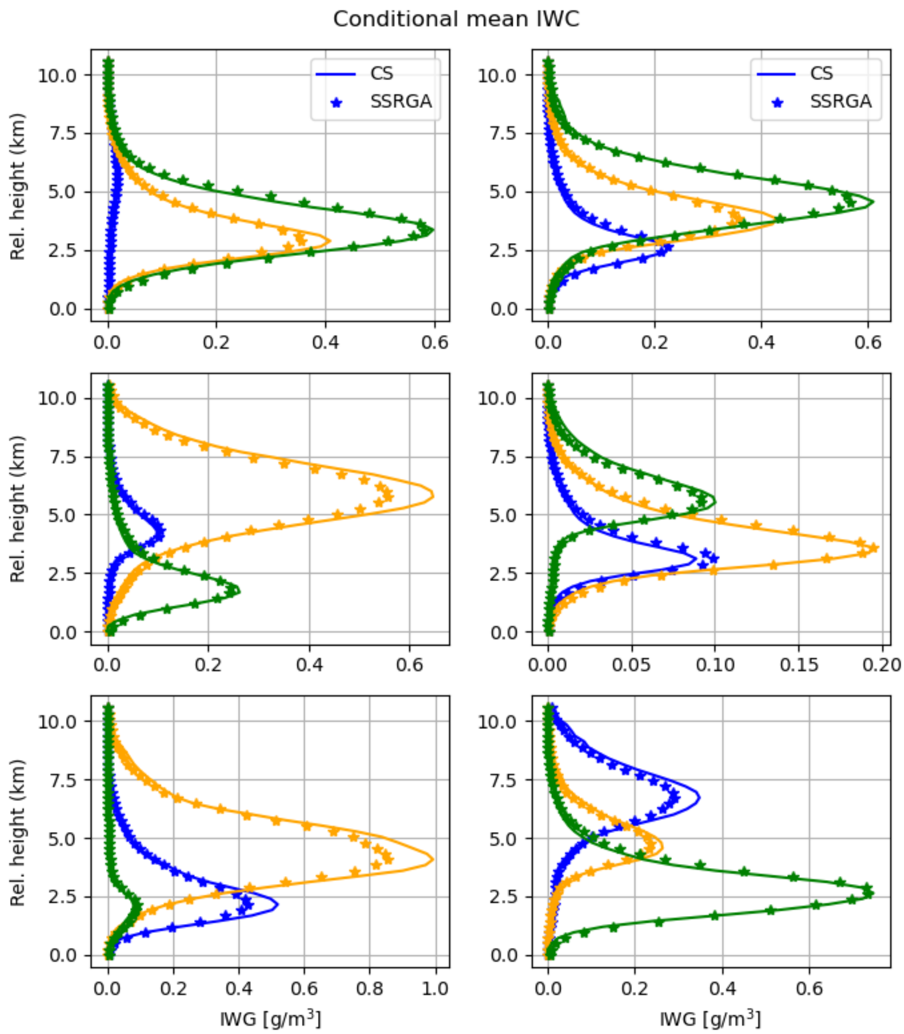

FIG. 1. Mean CS IWC profiles for 18 classes derived using the k-Means clustering algorithm. Associated mean profiles derived from CS reflectivity observations derived using SSRGA scattering calculations and N_w parameterization developed in this study are shown using symbol *. The vertical coordinate is defined relative to the freezing level

For the determination of reference a and b values to be used with Equation (1), we assume that PSDs are normalized gamma distributions with $N_w = 0.08 cm^{-4}$ and $\mu = 2$ and calculate

$$Z = \frac{\lambda^4}{\pi^5 |K_w|^2} \int_0^\infty N(D, D_m) \sigma_b(D) dD \tag{2}$$

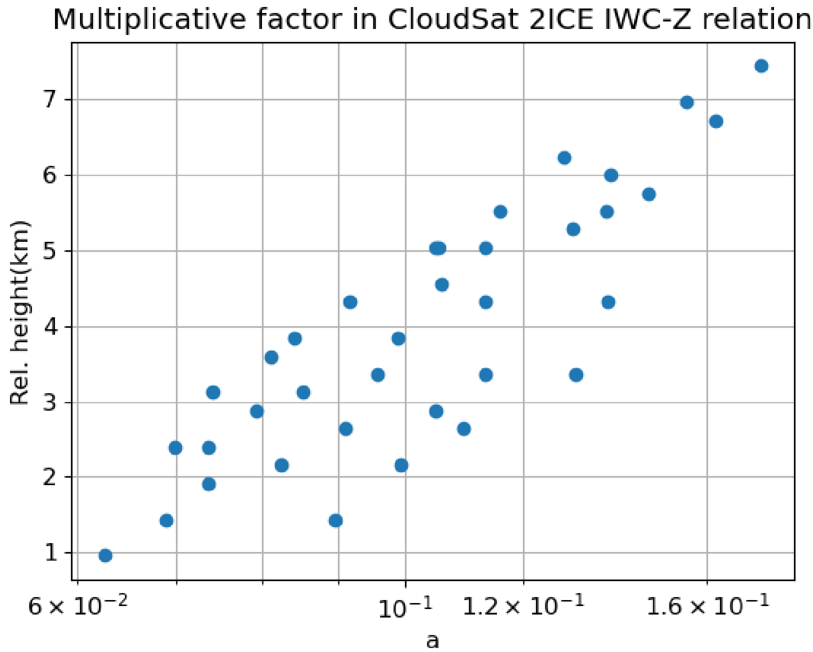

FIG. 2.

where λ is the radar frequency, $|K_w|$ is the dielectric factor of water, $N(D, D_m)dD$ is the number of ice particles of diameter with D and D+dD per unit volume, D_m is the mass weighted mean diameter of the distribution, and $\sigma_b(D)$ is the backscattering cross-section of ice particle of diameter D. The mass weighted mean diameter is equidistantly sampled to span the entire range of IWC values in the CS 2C-ICE dataset. The assumed mass-size relation is that of Brown and Francis (1995) because it works well with the SSRGA scattering calculations (Heymsfield et al. 2022). The open source software scatter-1.1 of Hogan (2019) is used to provide the actual scattering properties. The SSRGA theory was developed for millimeter and submillimeter-wave calculations and may not be applicable at lidar's wavelength. Therefore, for lidar calculations, we use the Mie solution included in the scatter-1.1 package. Although more accurate calculations based on more realistic ice particle shapes exist, they are rather incomplete and not readily available. Moreover, Wagner and Deleny (2022) compared lidar backscatter observations with backscatter calculations based on coincident PSD observations and the Mie solution and found good agreement, which suggests that electromagnetic properties derived from Mie calculations are adequate for practical applications. The lidar molecular backscatter and extinction are calculated using the lidar module of the CFMIP Observation Simulator Package (COSP; Bodas-Salcedo et al. 2011). To account for multiple-

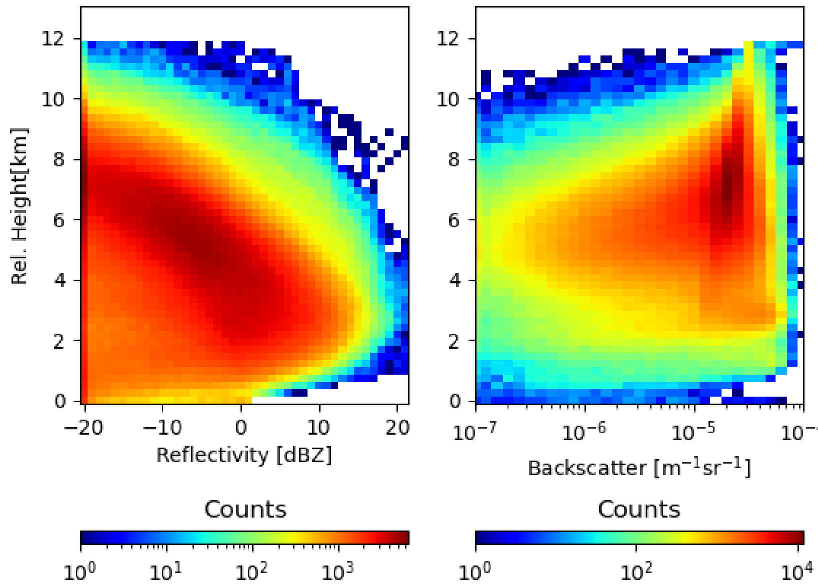

FIG. 3. Simulated distributions of Ku-band radar reflectivity (left) and lidar bacscatter (right) as function of height above the freezing level

scattering in the lidar observations, we are using the multiscatter-1.2.11 model (Hogan 2015) of Hogan and Battaglia (2008). Shown in Figure 3 are the distributions of simulated Ku-band radar reflectivity and lidar bacscatter as function of height above the freezing level.

The radiometer observations are calculated using a one-dimensional efficient, but accurate, radiative transfer solver based on Eddington's approximation (Kummerow 1993). The Eddington's approximation has been found to work well in cloud and precipitation retrieval application despite its simplicity relative to more general (but also computationally intensive) approaches such as the Monte Carlo radiative transfer solvers (Liu et al. 1996). It should be noted tough that the phase functions of ice particles tend to be highly asymmetric at sub-millimeter wave frequencies. For radiative transfer solutions based on the Eddington's approximation to be accurate it is necessary that the delta-scaling approach (Joseph et al. 1976) be employed. The delta-scaling approach transforms the initial radiative transfer equation into an equivalent one characterized by a less asymmetric scattering function and more extinction, which makes the solution Eddington approximation more stable and accurate. The absorption due to water vapor and other gases is quantified using the

Rosenkranz model (Rosenkranz 1998). The water vapor, temperature and pressure distributions are derived based on a WRF simulation of summer convection over the United States. Specifically, the water vapor, temperature and pressure profiles associated with times and areas where the model produces anvils are selected and clustered into 40 classes using the k-Means approach. The mean extinction profiles at the radiometer frequencies are calculated for every class and used in process of calculating the brightness temperatures from the estimated ice profiles using a simple Monte Carlo procedure. That is, given a retrieved ice profile and its scattering property, an anvil class and its associated absorption, temperature and pressure profiles are randomly selected and attached to the ice scattering properties. To make the procedure physically meaningful, temperature rather than height is used in the ice scattering-gas absorption collocation process. The emissivities are randomly chosen between 0.8 and 1.0 and assumed constant for all radiometer frequencies. Brightness temperatures are calculated at 89-, 183.31 ± 1.1, and 325.15 ± 1.5 GHz, which correspond to three of the 10 channels of the SAPHIR-NG radiometer envisioned to be deployed in the AOS mission (Brogniez et al. 2022). The other channels are centered on the same water vapor absorption lines and are not likely to offer additional information in this rather controlled experiment. Nevertheless, the other channels are expected to be useful in reducing the uncertainties caused by variability in the vertical distribution of water vapor, which may be greater in real life than in the simulated environment.

The processing steps used to process the CS reflectivity observations and calculate the lidar, Ku-band and submillimeter-wave radiometer observations may be summarized as follows:

1. Derivation of physically consistent radar and radiometer lookup tables to relate basic radar and radiometer properties (e.g. reflectivity, attenuation, extinction, scattering-albedo, etc.) to PSD parameters such as IWC and D_m. The tables are derived for a single of N_w, but are usable with any value of N_w using the "normalization" operations described in Grecu et al. (2011).

2. Derivation of Nw-relative height parameterization using the 2C-ICE product.

3. Estimation of IWC and related PSD parameters from CS W-band radar observations, using the tables constructed in Step 1 and parameterization derived in Step 2.

4. Calculation of lidar, Ku-band radar and radiometer observations from the estimates derived in Step 3 and the tables obtained in Step 1.

The application of these steps produces a large dataset of approximately 200,000 cloud ice profiles and associated lidar, radar and radiometer observations that may be used to investigate the synergy of the three sensors. Details are provided in the next section.

b. Estimation and evaluation

Given that the lidar observations may attenuate quickly in thick clouds, while the Ku-band radar will not detect clouds with an echo weaker than 8.0 dBZ, the radiometer is the instrument likely to provide by itself the most complete information about the total amount of ice in its observing volume. However, the vertical distribution of ice is difficult to quantify from radiometer-only observations, because significantly different ice vertical distributions may lead to very similar radiometer observations. This makes radiometer-only retrievals highly dependent on the ”a priori” information on the distribution of ice clouds in the atmosphere. As previously mentioned, this is the reason why CS-based IWC retrievals were preferred to CRM simulations, as retrievals are expected to result in more natural and less biased distributions.

We employ a two-step estimation methodology similar to that of Grecu et al. (2018). In the first step, we estimate the IWC class, out of the 18 classes of shown in Figure 1, to which the estimated IWC profile is most likely to belong. The class is estimated directly from the synthetic observations. In the second step, we estimate the IWC profile, using a class specific ensemble Kalman Smoother (EKS) methodology similar to that of Grecu et al. (2018). The EKS algorithm updates the estimated IWC relative to the mean IWC of the class to which the profile belongs. The differences between the actual active and passive observations and their mean class values are used in the update. The second step of this procedure is formally identical to the one used in Grecu et al. (2018), but the first step is different. In Grecu et al. (2018), the first step was based on a simple distance-based evaluation. That strategy is likely to be suboptimal in this study, because the joint distribution of IWC profiles and associated observations are significantly more complex. We therefore use a more complex classification methodology based on the TensorFlow library (Abadi et al. 2016). The class estimation model is defined as a TensorFlow Model with two dense layers of 30 neurons each, followed by a softmax layer (Goodfellow et al. 2016). The class estimation model is trained using the 70% of the simulated observations and the corresponding IWC profiles, the remaining 30% of the data being used for evaluation.

$$\mathbf{X} = \bar{\mathbf{X}}_\mathbf{i} + \mathbf{Cov}(\mathbf{X}_\mathbf{i}, \mathbf{Y}_\mathbf{i})\mathbf{Cov}(\mathbf{Y}_\mathbf{i}, \mathbf{Y}_\mathbf{i})^{-1}(\mathbf{Y} - \bar{\mathbf{Y}}_\mathbf{i}) \quad (3)$$

where $\mathbf{X}$ is the state variable describing the IWC profile, $\mathbf{Y}$ is the vector containing the variation, $\mathbf{X}_\mathbf{i}$ is the set of state variables for profiles in class i, and $\mathbf{Y}_\mathbf{i}$ is the set of associated observations. Variables $\bar{\mathbf{X}}_\mathbf{i}$ and $\bar{\mathbf{Y}}_\mathbf{i}$ are the mean values of the state variables and observations in class i, respectively. The covariance matrices between $\mathbf{X}_\mathbf{i}$ and $\mathbf{Y}_\mathbf{i}$ are denoted by $\mathbf{Cov}(\mathbf{X}_\mathbf{i}, \mathbf{Y}_\mathbf{i})$. In step 1, the class is estimated using the TensorFlow model, while in step 2, the IWC profile is estimated using the EKS algorithm summarized in Equation 3.

As already mentioned, a cross-validation methodology is used for evaluation, with 70% of the data used for training and the remaining 30% of the data used for validation. The partition of the data into training and evaluation subsets is done randomly. Usually, the partition, training and evaluation steps are repeated several times. However, given the fact that differences in the relationships between the ice property and their associated simulated observations are functions of the meteorological context, and that all regimes are well-sampled in both the training and testing subsets (e.g. out of every 10 pixels in a scene, about 7 end-up in the training dataset, while the others in the testing dataset), the repetition of the partition, training, and evaluation steps multiple times is not necessary. Therefore, in our evaluation, we partition the data into training and evaluation only once and perform all the evaluation for a single partition. The evaluation criteria include the correlation coefficient, the bias, and visual inspections of graphical representations of the estimated properties relative to their references.

3. Results

a. Radiometer-only retrievals

As previously mentioned, submillimeter-wave radiometers are likely to provide by themselves more complete information about the total amount of ice in their observing volumes than lidars or Ku-band radars with limited sensitivity. However, radiometers observations are an integrated measure of radiative process in clouds that provide little information about the vertical distribution of ice. From this perspective, an evaluation in terms of the ice water path (IWP) defined as the vertical integral of the IWC, i.e. $IWP = \int_0^{Z_{top}} IWC(z)dz$ is insightful. Shown in Figure 4 is the frequency of IWP estimated from radiometer-only observations as a function of its true value. As apparent in the figure, there is good correlation between the retrieved and the true IWP values. The numerical value of the correlation coefficient is 0.92, and there is no-overall bias. That is, the mean values of retrieved IWP and true IWP values are equal. However, conditional biases are apparent, with overestimation of IWP for values smaller than 100 g/m^2 and some underestimation for values larger than 1000 g/m^2. The biases at the low end of the IWP range are not surprising, given that the impact caused by ice scattering on the total radiometric signal is small for low values of IWP and hard to distinguish from other sources of variability in radiometer observations. Saturation effects are most likely responsible for underestimation at the high end. It should be noted that in this evaluation, only atmospheric profiles that exhibit ice detectable by the CS radar are used. Therefore, a radiometer-only estimation procedure derived from this training dataset is likely to result in significant overestimation if not used in conjunction with a discrimination procedure. However, such procedure is not critical in this study, as the lidar observations may be used to discriminate between clear skies and ice clouds. Although the radiometer-only estimation procedure is able to estimate the integrated amount of ice in clouds fairly wells, its ability to characterize the vertical distribution of ice in clouds is limited. Figure 5 shows the conditional vertical distributions of the estimated and true IWC for the 18 classes described in Section 2a and shown in Figure 1. As apparent in the figure, there are significant differences between the estimated and true IWC profiles.

Further insight into the radiometer-only estimation performance may be derived by defining the ice profile gravity center (GC) as $z_{GC} = \frac{\int_0^{Z_{top}} zIWC(z)dz}{\int_0^{Z_{top}} IWC(z)dz}$, where z is the distance relative to the freezing level, the Z_{top} is the distance from the top of the atmosphere to the freezing level. Shown in Figure 6 is the frequency of IWC gravity center estimated from radiometer-only observations as a function of its true value. It may be observed in the figure that while the true IWC gravity center exhibits quite a broad distribution, the one retrieved from the radiometer-only observations exhibits a multimodal narrow distribution. Moreover, there is almost no correlation between the retrieved and the true IWC gravity center. This is another indication that, while the total amount

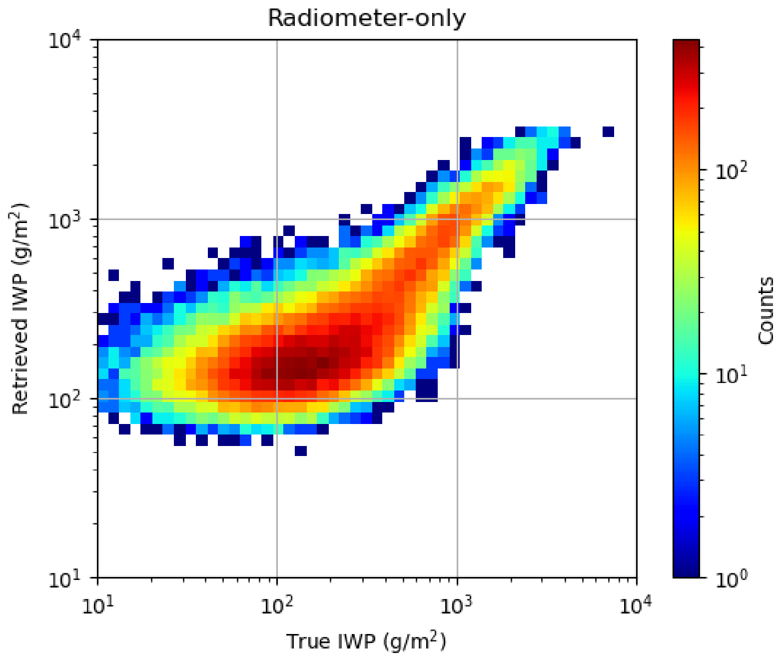

FIG. 4. Frequency plot of estimated IWP derived radiometer-observations as a function of the true IWP used in observations synthesis

of ice may be reasonably estimated from radiometer-only observations, its vertical distribution can not be determined from radiometer-only observations.

b. Synergistic retrievals

The synergy of the instrument on the estimates may be investigating by simply incorporating lidar and radar observations into the retrieval process and comparing the results with the radiometer-only estimates. Although the lidar observations are subject to attenuation, they are able to provide information about the vertical distribution of ice in clouds, especially at the top of the clouds. The radar observations, on the other hand, are able to provide information in the bottom part of the clouds, where the lidar signal is below the noise level due to attenuation. Therefore, the combined used of lidar and radar observations is expected to provide a more complete characterization of the vertical distribution of ice in clouds and enable the derivation of more specific estimates than those derived from radiometer-only observations.

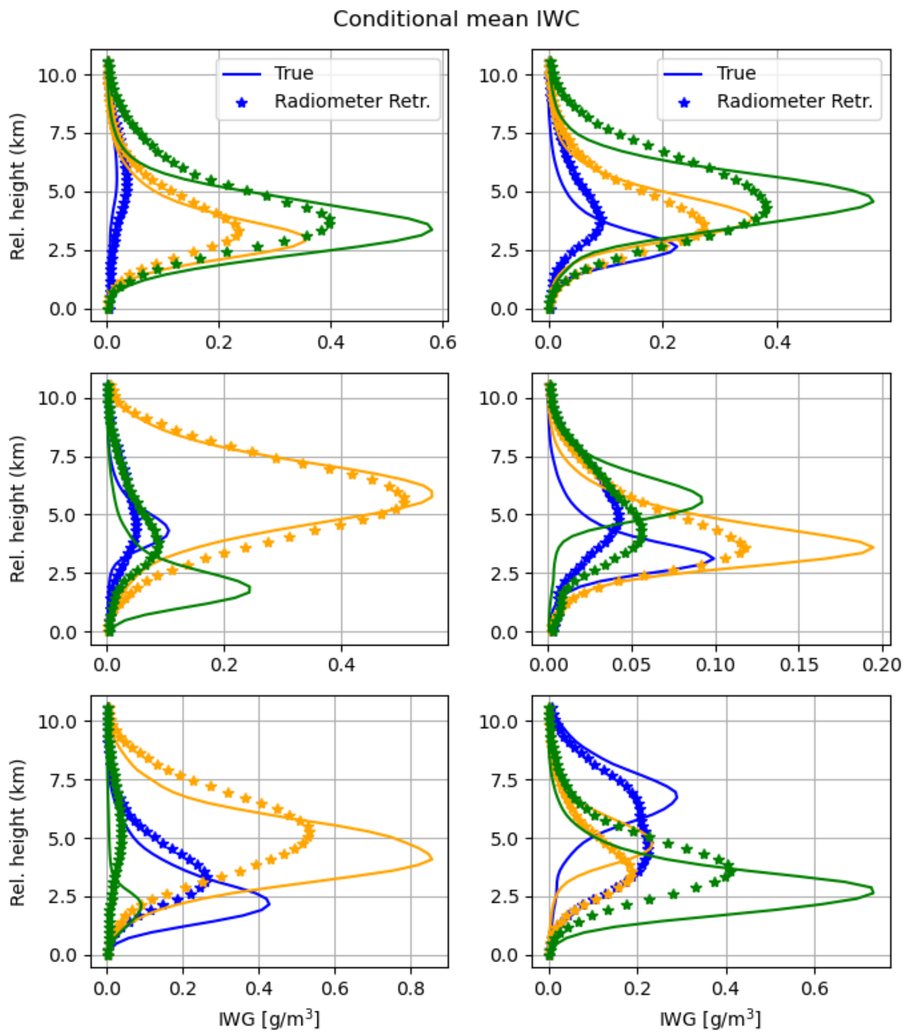

FIG. 5. True and radiometer-only retrieved conditional mean IWC for the 18 classes described in Figure 1.

Shown in Figure 7 is the distribution of the synergistic IWP estimates as a function of their true values. As apparent in the figure, the synergistic IWP estimates are more accurate than the radiometer-only estimates. At the same time, as apparent in Figure 8, the retrieved conditional mean IWC for the 18 classes described section 2a and shown in Figure 1 are in significantly better (almost perfect) agreement with the true IWC profiles than those derived from radiometer-only observations. Furthermore, as seen in Figure 8 the synergistic IWC gravity center estimates are in very good agreement with the true IWC gravity center.

While the estimates based on all instruments are significantly more accurate than those based on radiometer-only observations, it is useful to investigate how the two active instruments (lidar and

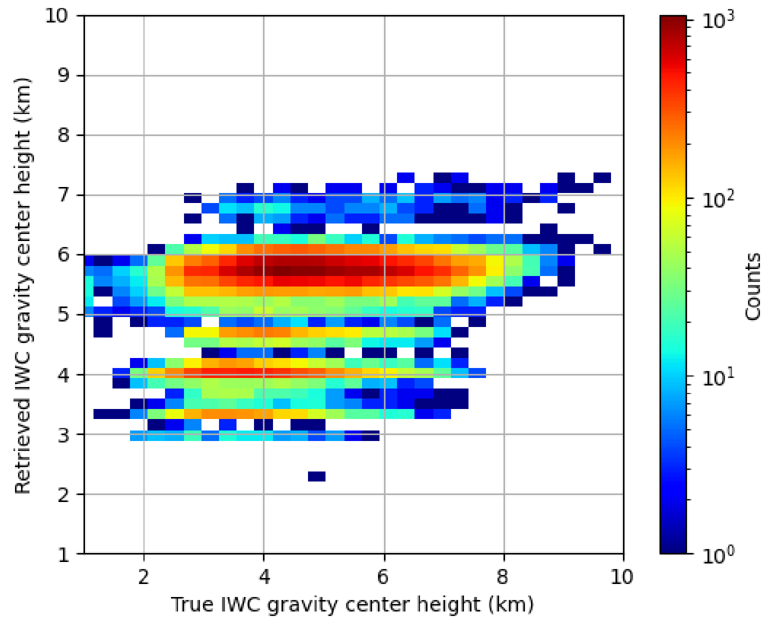

FIG. 6. Same as in Figure 4, but for the *IWC* gravity center.

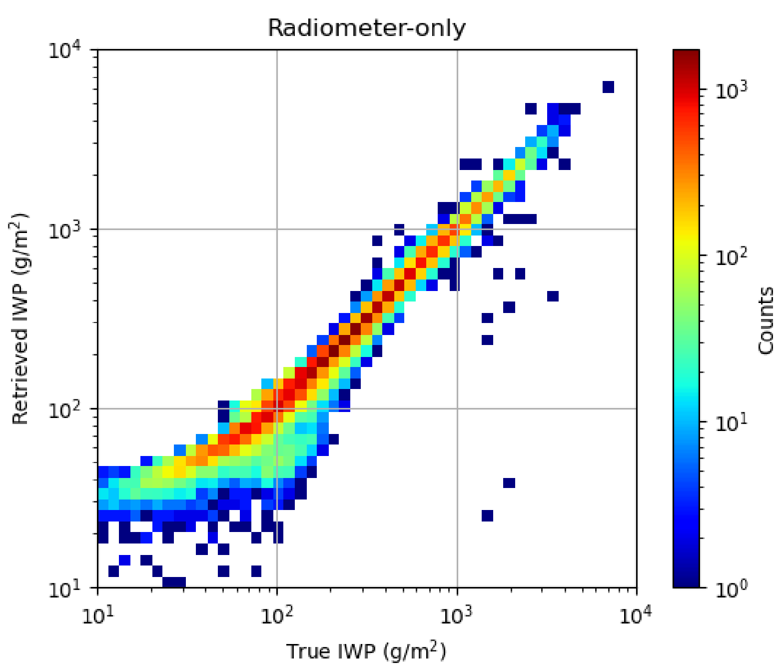

FIG. 7. Same as in Figure 4, but with the lidar and radar observations incorporated in the retrievals.

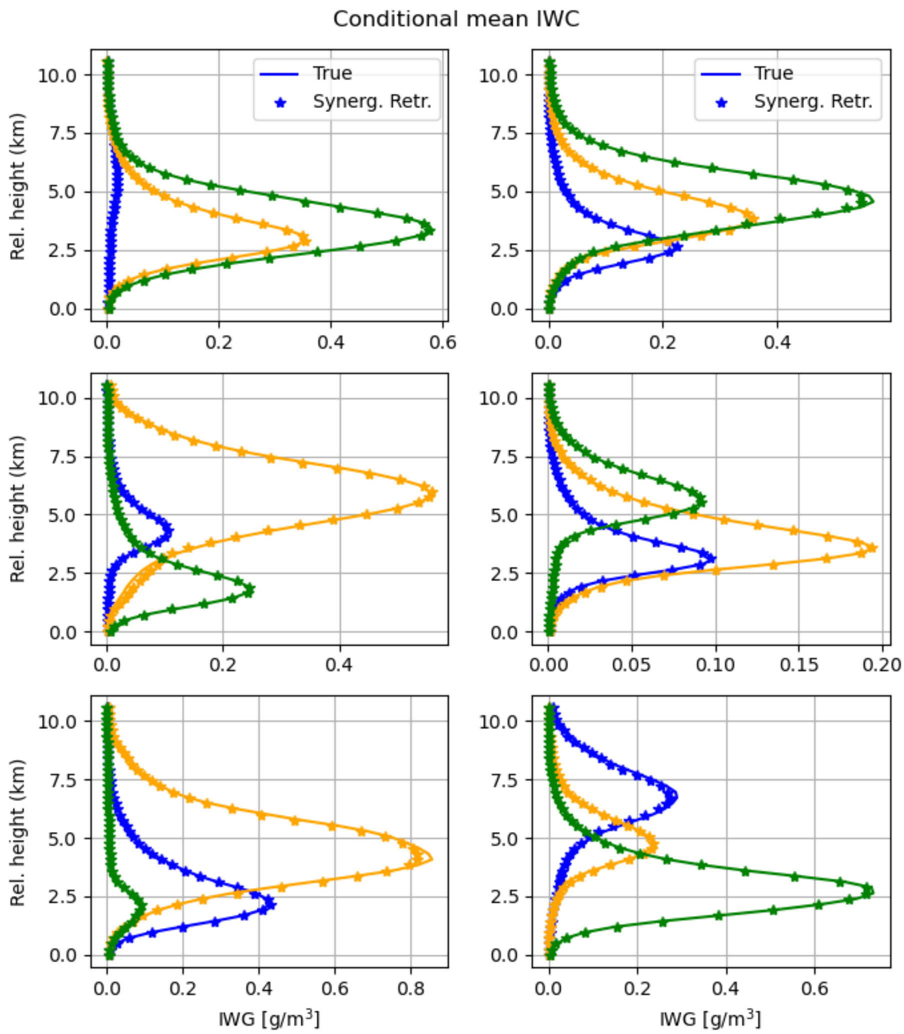

FIG. 8. Same as in Figure 5, but with the lidar and radar observations incorporated in the retrievals.

radar) impact the estimates. For conciseness, we used two statistical scores, namely, the normalized root mean square (NRMS) and the classification accuracy, to summarize the performance of the estimates. The NRMS is defined as

$$NRMS = \frac{\sqrt{\frac{\sum_{i=1}^{N}(IWC_i - IWC_{true,i})^2}{N}}}{\sqrt{\frac{\sum_{i=1}^{N}(IWC_{true,i} - \overline{IWC})^2}{N}}} \tag{4}$$

where IWC_i is the estimated IWP for the i-th sample, $IWC_{true,i}$ is the true IWC for the i-th sample, $\overline{IWC}$ is the IWC mean, and N is the size of the estimation dataset. The classification accuracy is

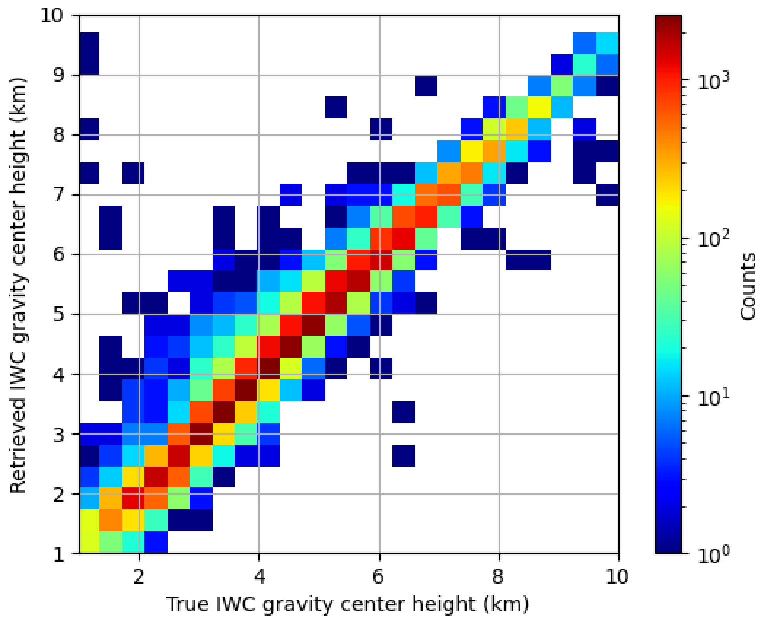

FIG. 9. Same as in Figure 6, but with the lidar and radar observations incorporated in the retrievals.

defined as

$$CA = \frac{\sum_{i=1}^{N} \delta_i}{N} \tag{5}$$

where δ_i is a binary variable that is equal to 1 if the estimated IWC class for the i-th sample is equal to the true IWC class for the i-th sample, and 0 otherwise. The performance summary is shown in Table 1 for several combinations of instruments. It may be observed in the table that the performance of the estimates based on all instruments is significantly better than those based on radiometer-only observations. Furthermore, the inclusion of the lidar observations in the retrieval process has a larger impact on the retrieval performance the inclusion of the radar observations. This is expected since the lidar observations are able to provide information about the top of the clouds, where the radar observations are above the noise level only occasionally. Nevertheless, the inclusion of the radar observations in the retrieval process has a notable impact on the accuracy of the IWC estimates relative to radiometer-only retrievals.

Table 1. Performance summary.

Score \ Instruments	Radiometer	Radar-Radiometer	Lidar-Radiometer	Radar-Lidar-Radiometer
NRMS	0.73	0.59	0.32	0.22
Class. Accurracy	0.39	0.48	0.92	0.94

4. Conclusions

In this study, we investigate the synergy of lidar, Ku-band radar, and sub-millimeter-wave radiometer measurements in the retrieval of the ice from satellite observations. The synergy is analyzed through the generation of a large dataset of IWC profile and the calculation of lidar, radar and radiometer observations using realistic models. The characteristics of the instruments (e.g. frequencies, sensitivities, etc.) are set based on the expected characteristics of instruments of the AOS mission. A cross-validation methodology is used to assess the accuracy of the retrieved IWC profiles from various combinations of observations from the three instruments. Specifically, the IWC and associated observations is randomly divided into two datasets, one for the training and the other for the evaluation. The training dataset is used to train the retrieval algorithm, while the evaluation dataset is used to assess the retrieval performance.

To ensure the self-consistency of results and their relevance to practical applications, the dataset of IWC profiles is derived from CloudSat reflectivity observations. Although subject to potential biases and uncertainties due to deficiencies in the retrieval models, these profiles are deemed to be more realistic than those derived from cloud resolving model simulations. Moreover, they are roughly consistent with the 2C-ICE CloudSat product (Deng et al. 2015), while relying on assumptions and parameterizations that enable the accurate computation of backscatter lidar, Ku-band radar, and sub-millimiter-wave radiometer observations.

The retrieval of the ice water content (IWC) profiles from the computed observations is achieved in two steps. In the first step, a class, out of 18 potential classes characterized by different vertical distribution of IWC, is estimated from the observations. The 18 classes are predetermined based on k-Means clustering algorithm. In the second step, the IWC profile is estimated using and Ensemble Kalman Smoother (EKS) algorithm that uses the estimated class as a priori information.

The results of the study show that the synergy of lidar, radar, and radiometer observations is significant in the retrieval of the IWC profiles. The inclusion of the lidar observations in the retrieval process has a larger impact on the retrieval performance than the inclusion of the radar observations.

Further work is necessary out to assess the impact of sources of uncertainties such as variability in the PSD intercept not captured by the current parameterization, differences in the instruments' footprint sizes, and non-uniform beam filling on the retrievals of the IWC profiles. Other sources of uncertainties that need be considered include the potential existence of supercooled liquid water in the clouds and uncertainties in the electromagnetic scattering properties used in the in instruments' forward models.

Acknowledgments. This work was supported by the NASA Remote Sensing Theory project through Grant 80NSSC20K1729. The authors thank Dr. Lucia Tsaoussi (NASA Headquarters) for her support of this effort.

Data availability statement.

References

Abadi, M., and Coauthors, 2016: Tensorflow: a system for large-scale machine learning. *Osdi*, Savannah, GA, USA, Vol. 16, 265–283.

Deng, M., G. G. Mace, Z. Wang, and E. Berry, 2015: Cloudsat 2c-ice product update with a new ze parameterization in lidar-only region. *Journal of Geophysical Research: Atmospheres*, **120 (23)**, 12–198.

Goodfellow, I., Y. Bengio, and A. Courville, 2016: *Deep learning*. MIT press.

Grecu, M., L. Tian, G. M. Heymsfield, A. Tokay, W. S. Olson, A. J. Heymsfield, and A. Bansemer, 2018: Nonparametric methodology to estimate precipitating ice from multiple-frequency radar reflectivity observations. *Journal of Applied Meteorology and Climatology*, **57 (11)**, 2605–2622.

MacKay, D. J., 2003: *Information theory, inference and learning algorithms*. Cambridge university press.